Research paper

Conversion reactions from dioctahedral smectite to trioctahedral chlorite and their structural simulations

Jie Meng[a,c], Xiaoyang Liu[a,b,*], Benxian Li[a,d,e,**], Juncheng Zhang[a], Daqian Hu[a], Jiuhua Chen[e], Weiguang Shi[f]

HPSTAR
591-2018

[a] College of Earth Sciences, Jilin University, 2199 Jianshe Street, Changchun 130012, China
[b] State Key Laboratory of Inorganic Synthesis and Preparative Chemistry, Jilin University, 2699 Qianjin Street, Changchun 130012, China
[c] College of Geographic Science, Harbin Normal University, 1 Shida Street, Harbin 150025, China
[d] Key Laboratory of Mineral Resources Evaluation in Northeast Asia, Ministry of Land and Resources of China, Changchun 130061, China
[e] Center for High Pressure Science and Technology Advanced Research, 2699 Qianjin Street, Changchun 130012, China
[f] Provincial Key Laboratory of Oil and Gas Chemical Technology, College of Chemistry and Chemical Engineering, Northeast Petroleum University, Daqing 163318, China

ABSTRACT

The clay minerals are good indicators of rock history because their wide transformation variations are sensitive to the formation conditions, like temperature (T), pressure (P) and fluid composition. Accordingly, many geothermometers and fluid-rock interaction indicators based on mineral assemblages, illite polytypism and composition of chlorite have been proposed during the last 30 years. In this study, dioctahedral smectite dominated mudstone was tested hydrothermally in the 250–550 °C temperature range and 5–280 MPa pressure range, with reactions lasting 24 h, with a liquid/solid ratio of 1:1, and in saturated KCl solution. The mineralogical and chemical evolution of the clay minerals was characterized by using X-ray powder diffraction (XRD), X-ray fluorescence spectroscopy (XRF), field-emission scanning electron microscopy (SEM), Fourier transform infrared spectroscopy (FTIR) and high resolution transmission electron microscopy (HRTEM). Molecular simulation was performed to determine the structure and behavior of interlayer cations and interlayer water changes of Na and Ca-rich smectite. We then obtained the transformation series as follows: from dioctahedral smectite to dioctahedral randomly interstratified illite/smectite to dioctahedral ordered illite/smectite to coexistence of dioctahedral and trioctahedral ordered illite/smectite and finally to trioctahedral chlorite and illite/smectite. This work illustrated the dioctahedral smectite alteration and transformation process and showed a continuous octahedral sheet transformation from dioctahedral smectite to trioctahedral chlorite. The series of clay minerals transformation provided an important experimental basis for understanding the geochemical conditions to which clay minerals were exposed to in the geological environment and will offer basic parameters for establishing a quantitative link between composition and formation conditions.

1. Introduction

Phyllosilicates exist in a wide variety of environments and rock types including volcaniclastic sediments, altered igneous rocks, and pelitic rocks which have gone through a diagenetic and a very-low-grade to low-grade metamorphism (Merriman and Peacor, 1999). Mineralogic reactions in phyllosilicates, particularly the low-temperature conversion of dioctahedral smectite to illite and trioctahedral smectite to chlorite, have attracted much interest in recent years. These two mineral transformations can be applied as a geothermometer and as an indicator of fluid-rock interaction. The reaction of dioctahedral

smectite to illite (S → I) occurs under increasing temperature during the burial process and is considered temperature dependent when adequate amounts of K⁺ ions are available (Dong et al., 2002). During the burial process, fine-grained sediments at low temperatures are usually rich in smectite, while deeply buried mud rocks are rich in illite (Burst, 1969; Perry Jr and Hower, 1972). The other transformation of trioctahedral smectite to chlorite (S → C) is also one of the most fundamental reactions in diagenesis and low-grade metamorphism of intermediate to mafic volcanic rocks and volcanogenic sediments (Murakami et al., 1999). The trioctahedral smectite-to-chlorite conversion has been characterized both as continuous with a gradual decrease in percentage

of smectite (%S) (e.g., Chang et al., 1986; Bettison and Schiffman, 1988; Bevins et al., 1991) and as discontinuous with a stepwise decrease in % S (e.g. Inoue et al., 1984; Inoue and Utada, 1991; Schiffman and Staudigel, 1995; Murakami et al., 1999; Robinson and Zamora, 1999). Continuous conversion suggests the presence of randomly interstratified C/S whereas discontinuous conversion suggests its absence.

It is increasingly being recognized that phyllosilicates reactions exist not only in the burial and low-temperature metamorphism, but also in the subduction zones or slip faults. The characterization of clay minerals has also proved of interest to better understand fault tip propagation in crustal fault-zone or in subduction regions (Ferrage et al., 2011). Phyllosilicate diagenetic reactions release fluids (e.g., the smectite-illite transformation) (Vidal and Dubacq, 2009; Dubacq et al., 2011), that have a direct effect on the mechanical coupling process along the plate interface (Kameda et al., 2011) or it can have a strong impact on the rock rheology as fluid pressure can reduce the effective stress state and promote slip formation. However, the mineralogic properties of fault-related rocks can similarly affect fault behavior by inducing weak mineral phases at the interface (Schleicher et al., 2012). In the cores collected from the SAFOD project in Parkfield, California, and localized in fault-rock samples, the presence of smectite clay minerals has increasingly been confirmed as evidence for mineralogic weakening (Schleicher et al., 2006; Schleicher et al., 2010; Bradbury et al., 2011; Holdsworth et al., 2011).

Phyllosilicate transformations occur as a response to the burial process and are mainly controlled by temperature (T), pressure (P), time, and some chemical variables (Ferrage et al., 2011). When the faulting process starts, frictional heating induces a slight temperature rise, influencing pore fluid properties and geochemical bearing fluids along numerous faults (e.g., K^+) and makes the transformation of clay minerals become more complicated and slightly quicker than the normal burial-diagenetic or low-grade metamorphism (Abid et al., 2004; Kameda et al., 2011). However, the multiple transformation modes of clay minerals are probably related to specific environmental conditions that are not yet clearly defined. For these reasons, hydrothermal laboratory experiments are essential to assess the main parameters controlling the extent of illitization and chloritization as well as those that could lead to a better understanding of the series of transformation.

Traditionally, it has been considered that there is a compositional gap between dioctahedral and trioctahedral structures and there is no continuum in the composition of the octahedral sheet between the two groups (Cuadros, 2012). Therefore, the mechanisms that transform dioctahedral smectite into illite via interstratified illite/smectite (I/S) and trioctahedral smectite transformation into chlorite via interstratified chlorite/smectite (C/S) or corrensite are widely accepted by geoscientists. Numerous results are available from the literature on the experimental behavior of smectites under hydrothermal conditions, generally in the presence of chloride solutions (Eberl, 1978; Eberl et al., 1978; Yamada et al., 1998), however, compared to the amount of research effort devoted to the transformation of dioctahedral smectite to illite, studies about the transformation of dioctahedral smectite to trioctahedral chlorite or chlorite/smectite are still limited. The limited observations of dioctahedral smectite transforming into trioctahedral chlorite or chlorite/smectite can be attributed to the different chemical environments (Hillier and Velde, 1992) and the phase transformation of clay minerals under low temperatures, and the long burial time the transformation needs.

The main aim of this work is to investigate in detail the transformation process of dioctahedral smectite at the same liquid/solid (L/S) ratios, both through experiments and the simulation of the behavior at the atomic level in clay-mineral structural models by molecular simulations. Hence, dioctahedral Na, Ca-smectite-rich mudstones that originated from the Jiufengshan formation in the Dayangshu basin, east of Inner Mongolia in China were selected as the starting material. A continuous octahedral sheet transformation from dioctahedral smectite to trioctahedral chlorite was obtained: from dioctahedral smectite to dioctahedral randomly interstratified illite/smectite to dioctahedral ordered illite/smectite to coexistence of dioctahedral and trioctahedral ordered illite/smectite and finally to trioctahedral chlorite and illite/smectite.

2. Experimental

2.1. Sample collection

To clarify clay mineral transformation process on the history of diagenesis, very-low grade and low-grade metamorphism in the area, dioctahedral Na, Ca-smectite dominated mudstone was selected as the starting material. The mudstone was originated from the Mesozoic Jiufengshan formation in the Dayangshu basin, located in the Arong Banner and Oroqen Banner, east of Inner Mongolia, with the geographic coordinates of 124°23′39.7″E, 50°01′14.7″N. They were influenced by early diagenesis processes and the temperature estimated for the diagenetic changes was below 100 °C. The mudstone was crushed in an agate mortar and directly studied by XRD. The analysis of the randomly oriented powder XRD showed that the primary mineral components were smectite with a small amount of muscovite, quartz and feldspar. The fractions separated from the uppermost part of the suspension were noted to contain smectite (± 95%) and a small amount of illite and muscovite. The chemical composition of the fractions, as determined by X-ray fluorescence (XRF) method using a PANalytical AXIOS spectrometer, is shown in Table 1. Calculated on the base of O_{11}, the half structural formula of the suspension was: $(Ca_{0.143}Na_{0.137}K_{0.124}Mg_{0.073})_{0.477}(H_2O)_n\{(Al_{1.594}Mg_{0.246}Fe_{0.122}Ti_{0.038})_{2.00}[(Si_{3.515}Al_{0.485})_{4.000}O_{10}](OH)_2\}$. There were some substitutions of Al^{3+} for Si^{4+} in the tetrahedral sheet.
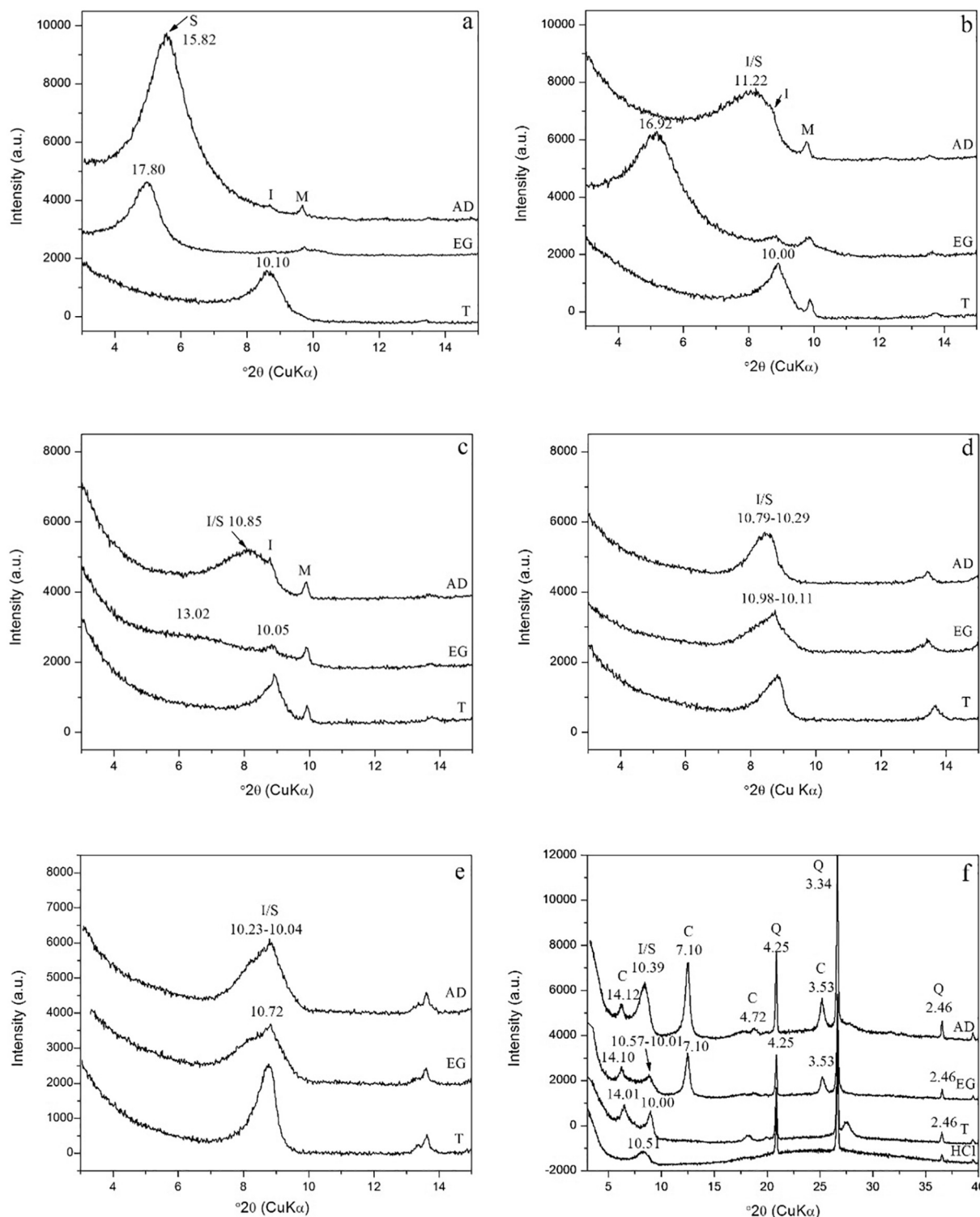
2.2. Hydrothermal experiments set-up

Weighed 0.2 g hand-crushed powder of mudstone samples, and then sealed them into a 2.5 cm long Ag capsule with a diameter of 0.5 cm. 0.2 ml [liquid/solid ratio (L/S) = 1:1] of saturated potassium chloride (KCl) solution was added into each capsule, and the capsules were sealed up at both ends and then loaded into the high-pressure autoclave. To increase the reaction rate, we increased the temperature and pressure to above that reported in the literature (smectite transformed to illite at about below ~180 °C, mixed-layer chlorite/smectite to 240 °C in the Nesjavellir geothermal field in Iceland). The experiments were conducted using a LECO hydrothermal apparatus (HR-1B-2-847, LECO Corp., US) with different conditions: 250 °C and 5 MPa, 350 °C and 65 MPa, 450 °C and 120 MPa, 550 °C and 265 MPa, 550 °C and 280 MPa, and each was maintained for 24 h. The temperature control was precise to ± 1 °C and accurate to ± 5 °C. The relative samples are labeled as 1-250-5-KCl-24, 1-350-65-KCl-24, 1-450-120-KCl-24, 1-550-265-KCl-24 and 1-550-280-KCl-24, respectively. The reacted material and the solution were separated by centrifugation. To exclude excess electrolytes in the products, the obtained products were washed several times with deionized water until chloride-free (this was tested by using $AgNO_3$ solution), then dried at 60 °C and grounded before characterization.

Table 1
The chemical composition (in mass %) of smectite.

SiO₂	Al₂O₃	Fe₂O₃	TiO₂	CaO	MgO	K₂O	Na₂O
58.523	29.367	2.698	0.834	2.218	3.563	1.621	1.177

Fig. 1. XRD patterns for < 2 μm fractions of the primitive rock (a) and the samples after a series of reaction at different conditions: (b) 250 °C, 5 MPa, 24 h; (c) 350 °C, 65 MPa, 24 h; (d) 450 °C, 120 MPa, 24 h; (e) 550 °C, 265 MPa, 24 h; (f) 550 °C, 280 MPa, 24 h, respectively. The diffraction peaks arising from (a) smectite sample with peak labeled as S and a small amount of illite and muscovite with peak labeled as I and M. (b), (c) Sample with illite/smectite (I/S), and a small amount of illite (I) and muscovite (M). (d) and (e) Sample with illite/smectite (I/S). (f) Sample with chlorite (C), illite/smectite (I/S), and quartz (Q). The main peaks from the experimental patterns are labeled in Å. AD (air-dried), EG (ethylene glycol) and T (heated to 550 °C).

2.3. Characterization

2.3.1. X-ray powder diffraction (XRD)

Oriented XRD patterns were collected from 3° to 40° (2θ) at a scanning rate of 2° (2θ) min^{-1} using a Rigaku D/Max2550 V/PC X-ray diffractometer, with graphite-monochromated Cu Kα radiation (λ = 1.5418 Å), operating at 50 kV and 200 mA. To analyze the d_{060} region, randomly oriented powder XRD patterns were collected from 57° to 65° (2θ) at a scanning rate of 1° (2θ) min^{-1} using the same instrument as mentioned above.

To obtain oriented samples, the raw and experimental samples were crushed with an agate mortar. The powder was then disaggregated in distilled water using an ultrasonic bath. After 20 min of ultrasonic processing, suspensions of the clay fraction were pipetted and deposited onto glass slides. Clay minerals in this fraction were identified according to the position of the basal reflections on XRD patterns of air-dried (AD) slides, ethylene-glycolated (EG) slides and heated (550 °C for 2.5 h in the air, T) slides. Additionally, to verify the existence of chlorite, some samples were treated by hydrochloric acid with the concentration of 6 mol/l and extracted into an 80 °C water bath for 15 min. The products were then washed several times with the distilled water until chloride-free after cooling to room temperature and tested using $AgNO_3$ solution. Finally, the suspensions of the prepared samples were smeared onto glass slides and dried at room temperature to obtain hydrochloric acid (HCl) treated samples. The clay mineral determination and related quantitative analysis were based on the comparison of the diffraction peak positions and intensity to the standard of the Petroleum Industrial Standard (SY/T5163-2010) and Srodon (1984).

2.3.2. X-ray fluorescence spectroscopy (XRF)

Major element analysis was conducted with an AXIOS X-ray fluorescence spectroscope (XRF) with Phillips Super Q software. Samples were ground by hand using an agate mortar and pestle to pass 200 mesh, after which the clay fraction was separated from the uppermost part of the suspension and dried in the air. The dried fraction of the samples was measured in boric acid pellets and the pellets were prepared with a pelletizer at 10 MPa. Each sample was measured at least three times.

2.3.3. Field-emission scanning electron microscopy (FE-SEM)

SEM images were recorded using a JEOL JSM 6700F field emission scanning electron microscope (FESEM, JSM6700F, JEOL, Japan) at 5.0 kV accelerating voltage and working distance (WD) of 8.1 mm.

2.3.4. Fourier transform infrared spectroscopy (FTIR)

The FTIR spectra were obtained with a Bruker IFS-66V/S Fourier transform infrared spectrometer using the KBr pressed disk technique. To obtain a well-proportioned mixture, each sample was prepared with a clay/KBr ratio of approximate 1:100, and ground in an agate mortar for 10 min. The mixture was then heated under a lamp for 3 min to minimize water adsorption before FTIR measurements. The spectra were collected over the range of 4000–400 cm^{-1} with a resolution of 4 cm^{-1}.

2.3.5. HRTEM analysis

For lattice fringe image observation, the air-dried clay samples (1-550-280-KCl-24) were impregnated in resin and cut by ultramicrotomy to create thin films of < 150 nm in thickness. This process approximately aligns the c* axes of sheet silicates normal to the electron beam. The thin films were placed onto copper TEM grids and examined on JEOL FEI Tecnai G2 S-Twin F20.

2.3.6. Materials studio (MS) simulation

To intuitively display the transformation process of smectite to chlorite on a molecular level, molecular modeling and molecular simulation were introduced to simulate the mineral and structure changes. For the reason that interlayer water was present in the structure of smectite, in the process of MS simulation, the space group of P1 was required when sorption calculation was used to add interlayer water into interlayer space. Smectite models were based on a space group P1 (Viani et al., 2002). The cell units were built by inputting the parameters: α = β = γ = 90°, a = 5.18 Å, b = 8.98 Å and c = 15.00 Å. Illite models were based on a space group of C2/m (Gualtieri et al., 2008). The cell units were built by inputting the parameters: α = γ = 90°, β = 101.11°, a = 5.189 Å, b = 8.953 Å and c = 10.129 Å. Chlorite models were based on a space group of C2/m (Zheng and

Bailey, 1989). The cell units were built by inputting the parameters: α = γ = 90°, β = 96.82°, a = 5.328 Å, b = 9.228 Å and c = 14.363 Å. To obtain a reasonable size for the model, three 2a × 2b × 2c supercells and their simulated powder XRD patterns were created.

3. Results

3.1. XRD of the clay fraction

3.1.1. XRD of oriented samples

Clay minerals identified in the fraction are shown in Fig. 1. Smectite, mixed-layer minerals I/S and chlorite are the clay phases identified in the samples. In each of the diffraction patterns, three patterns were labeled as AD (air-dried), EG (ethylene glycol) and T (heated to 550 °C), respectively. By combining those three diffraction patterns, the features of clay minerals can be clearly characterized. The diffraction patterns of the primitive rock (labeled as 1-YY) were shown in Fig. 1a. As is shown, a characteristic clay mineral peak occurred with a spacing of ~15.0 Å. After the solvation of ethylene glycol, the ~15.0 Å peak of the AD samples disappeared, while a ~17.0 Å peak appeared. The ~15.0 Å peak completely collapsed to 10 Å after high temperature treatment. Consequently, these changes indicated that smectite-dominated clays occurred in the initial materials, and due to some organic matter in the interlayer, the d value of ~15.0 Å reflections appeared a little larger, as shown in Fig. 1a, it was 15.82 Å. Illite and muscovite were identified using 10.0 Å and 9.12 Å reflections, respectively (In Fig. 1a the two phases were denoted as I and M). After a series of hydrothermal experiments, the corresponding XRD patterns are shown in Fig. 1b–f. As shown in Fig. 1b–e, the characteristic clay mineral peak occurred with a spacing of 10–15.0 Å in the XRD patterns for each specimen in the AD slides. After the solvation of ethylene glycol, the 10–15.0 Å peaks of the AD samples expanded to ~17.0 Å in the EG slides, as shown in Fig. 1b. However, a large bulge of about 13.02 Å formed while ~17 Å reflection peak disappeared in the EG slides of Fig. 1c. These results indicated that the interstratified I/S transformed from disordered interstratified minerals to ordered interstratified minerals (Srodon, 1980; Watanabe, 1981; Velde et al., 1986; Watanabe, 1988). The diffraction peaks in the EG slides shifted slightly to lower 2θ angles and became a little broader compared with those of the AD slides in Fig. 1d and e. It showed that the final samples still contained a small amount of smectite layer. The muscovite disappeared at this point in Fig. 1d and e. Additionally, in Fig. 1b–e, the diffraction peaks with a d value of 10–15.0 Å in the AD slides from our experiments completely collapsed to 10 Å after they were treated with high temperature.

As is shown in Fig. 1f, the peak with a d value of 14.12 Å appeared in the AD slides. However, after the solvation of ethylene glycol, that diffraction peak remained stable at 14.10 Å, and then shifted to 14.01 Å after the slide was treated by high temperature. These results indicated that chlorite may have appeared. To further confirm the appearance of a chlorite layer, the products were treated with dilute hydrochloric acid and then smeared onto a glass slide. This approach can be used to distinguish chlorite and kaolinite owing to the similar diffraction peaks with d values of 7.20 and 3.58 Å between those clay minerals. Common trioctahedral chlorite can dissolve in hot hydrochloric acid, while kaolinite cannot (Zhao and He, 2016). As was shown, the disappearance of 14.12, 7.10, 4.72, 3.53 Å peaks could be attributed to chlorite (Fig. 1f). Thus, these results showed that chlorite (C) clays formed, while a small amount of illite/smectite (I/S) layers remained in the final products. Furthermore, we had gained the transformation series of clay minerals from smectite to randomly interstratified I/S, then to ordered interstratified I/S, to chlorite and I/S. Because of these results, we can also conclude that chlorite can form from smectite and illite/smectite.

3.1.2. XRD of randomly oriented samples

In the previous studies of XRD patterns for clay minerals, the $d_{(060)}$ of 1.48–1.50 Å indicated a dioctahedral phase, and the spacing of
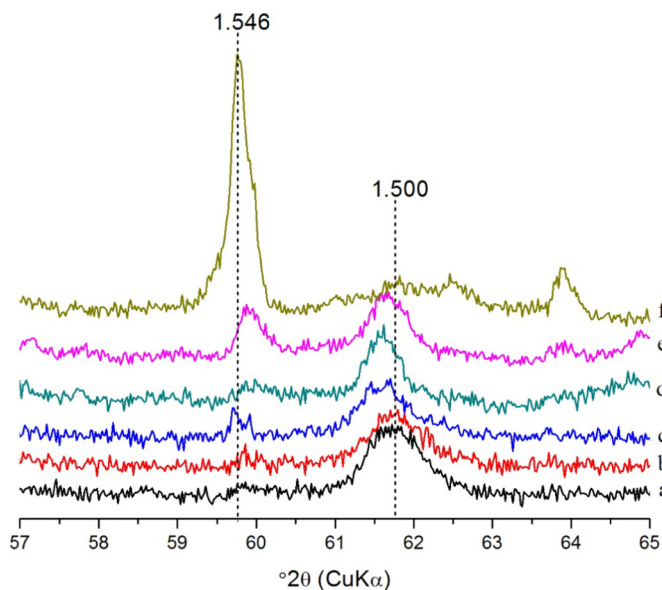
Fig. 2. Comparison of XRD patterns of the position of the (060) peak, (a) 1-YY, (b) 1-250-5-KCl-24, (c) 1-350-65-KCl-24, (d) 1-450-120-KCl-24, (e) 1-550-265-KCl-24, (f) 1-550-280-KCl-24, *d*-spacing values are in Å.

1.53–1.55 Å indicated a trioctahedral phase (Brindley and Brown, 1980). The XRD patterns of Fig. 2 showed that a broad peak near 1.500 Å appeared in the diffraction patterns of the samples of 1-YY (Fig. 2a), 1-250-5-KCl-24 (Fig. 2b), 1-350-65-KCl-24 (Fig. 2c), and 1-450-120-KCl-24 (Fig. 2d), while, the two diffraction peaks with the spacing of ~1.543 Å and ~1.500 Å appeared in the XRD patterns of 1-550-265-KCl-24 (Fig. 2e). In the sample of 1-550-280-KCl-24 (Fig. 2f), the intensity of the spacing of 1.500 Å decreased significantly, while showing strong peaks of 1.546 Å. Thus, the results indicated that the trioctahedral clay minerals formed after the gradual transformation from dioctahedral-dominated structures to dioctahedral-trioctahedral-dominated mineral structures and then to trioctahedral-dominated structures. It indicated that with the increasing of temperature and pressure, Al^{3+} and Fe^{3+} of dioctahedral minerals were altered by Fe^{2+} and Mg^{2+} in octahedral structures, and the transformation of the clay mineral structures from dioctahedral-dominated to trioctahedral-dominated species.

3.2. Geochemical changes of samples before and after reaction

The chemical compositions of clay minerals in primitive rock (1-YY) and in experimental samples (1-250-5-KCl-24, 1-350-65-KCl-24, 1-450-120-KCl-24, 1-550-265-KCl-24 and 1-550-280-KCl-24) were determined by XRF (Table 2). The structural formulas of all samples were calculated for O_{10} $(OH)_2$, except for sample 1-550-280-KCl-24. In sample 1-550-280-KCl-24, due to the coexistence of chlorite and illite/smectite (I/S) (as shown in Fig. 1f), the structural formula was calculated for both O_{10} $(OH)_2$ and O_{10} $(OH)_8$, respectively.

As is shown in Table 3, the content of the interlayer cation K^+

gradually increased with the rise of temperature and pressure. This phenomenon is in good accordance with XRD patterns. With the increase of temperature and pressure, the interlayer cations (Ca^{2+}, Na^+, and Mg^{2+}) were substituted by cation K^+. In the samples 1-450-120-KCl-24 and 1-550-265-KCl-24, as is shown in Fig. 1d and e, illite was the dominant mineral phase and the content of the interlayer cation K^+ reached the maximum (Table 3). Exchange between the interlayer cations and K^+ was accompanied by a slight increase of interlayer charge, except for the samples of 1-350-65-KCl-24 and 1-550-280-KCl-24 (Table 3). The temperature of 350 °C was always considered to be within the range of the thermal decomposition of organic matter (Boyle, 2004), and the release of organic matter may affect the crystallite of clay minerals, so the organic matter may affect the conversion reactions in the conditions of 350 °C 65 MPa. As shown in Fig. 1f, the sample of 1-550-280-KCl-24 contained clay minerals of chlorite and illite/smectite. The newly formed chlorite contained a lesser content of K^+ compared to that of illite. The exchange of cations in the octahedral sheet led to the reduction of mineral interlayer charge. This trend of variation was in good agreement with the corresponding XRD patterns in Fig. 1. Accordingly, it suggested that major element changes, except for Al ions, were in accordance with the successive transformation series of clay minerals: from smectite to randomly interstratified I/S, then to ordered interstratified I/S, to chlorite and amounts of I/S shown in the hydrothermal experiments. In this paper, the experiments of clay mineral transformation were carried out in a closed system, therefore, the quartz was inevitably generated as a byproduct and retained after the purification process of clay minerals. Thus, this would affect the analysis of the content of SiO_2 more than that in pure clay minerals. The tetrahedral layer was filled with Si and sufficient Al to occupy the four sites, considering Al ions was conserved, the content of Al ions that were assigned to the octahedral layer would be more than that of a realistic mode in a crystal formula.

3.3. Morphology of selected samples

SEM imaging of the rock fragments 1-YY showed smectite with pseudohexagonal and flaky shapes ranging between 1 and 4 μm in basal length (Fig. 3a). However in Fig. 3b, the SEM imaging of the sample of 1-550-265-KCl-24 showed coarse grained flaky shapes of < 2 μm in basal length. At this condition, the sample should consist of illite and a small amount of smectite (6%). Moreover, the imaging of the sample of 1-550-280-KCl-24 dominantly consisted of chlorite and illite/smectite, showed pseudohexagonal and flaky shapes of < 2 μm in basal length (Fig. 3c). In summary, these grains presented a characteristic sign of particle smectite dissolution with irregular crystal edges as well as recrystallization to form the illite and chlorite.

3.4. FTIR analysis of clay mineral

Typical FTIR spectra together with band vibration wavenumbers in the regions of 4000–3300 and 1300–400 cm^{-1} were shown in Fig. 4. In the OH-stretching region of 3800–3500 cm^{-1}, absorptions at ~3620 cm^{-1} were ascribed to OH-stretching that was bonded to Si-O-Si linkage in the octahedral sheet, corresponding to aluminous minerals

Table 2
Average major-element composition (in wt%) of the 1-YY and hydrothermal samples, from XRF analysis.

Sample	Main clay minerals	SiO_2	Al_2O_3	MgO	Fe_2O_3[a]	TiO_2	CaO	Na_2O	K_2O
1-YY	Smectite-dominated	58.523	29.367	3.563	2.698	0.834	2.218	1.177	1.621
1-250-5-KCl-24	I/S-dominated	56.021	29.584	3.108	3.158	1.090	0.928	0.694	5.417
1-350-65-KCl-24	I/S-dominated	58.014	30.163	3.086	1.326	0.904	0.815	0.587	5.103
1-450-120-KCl-24	I/S-dominated	56.307	28.275	2.439	1.222	0.964	0.823	0.754	9.216
1-550-265-KCl-24	I/S-dominated	56.559	27.284	2.560	1.902	1.044	0.749	0.733	9.168
1-550-280-KCl-24	Chlorite and I/S dominated	61.067	28.389	3.085	2.239	0.890	1.861	0.581	1.886

[a] Total Fe expressed as Fe_2O_3.

Table 3
Average structural formulas of the 1-YY and hydrothermal samples.

Sample	Si	^{IV}Al	^{VI}Al	^{VI}Mg	^{VI}Fe^{3+}	^{VI}Ti	Mg int	Ca	Na	K	Sum of interlayer cation charge
1-YY	3.515	0.485	1.594	0.246	0.122	0.038	0.073	0.143	0.137	0.124	0.693
1-250-5-KCl-24	3.437	0.563	1.576	0.228	0.146	0.050	0.056	0.061	0.083	0.424	0.741
1-350-65-KCl-24	3.516	0.484	1.671	0.228	0.060	0.041	0.051	0.053	0.069	0.395	0.672
1-450-120-KCl-24	3.508	0.492	1.584	0.227	0.057	0.045	0	0	0.059	0.733	0.792
1-550-265-KCl-24	3.530	0.470	1.537	0.238	0.089	0.049	0	0	0.052	0.730	0.782
1-550-280-KCl-24[a]	3.640	0.360	1.634	0.226	0.100	0.040	0.048	0.119	0.067	0.143	0.544
1-550-280-KCl-24[b]	4.000[c]	0	2.538	0.349	0.128	0.051	0	0.151	0.085	0.183	0.570

[a] Base on O$_{11}$.
[b] Base on O$_{14}$.
[c] Apparent excess silica was subtracted.

such as kaolinite, smectite or illite (Hong et al., 2014). The FTIR spectra of I/S show Si—O bending, stretching and OH-bending absorptions in the 1300–400 cm^{-1} region. The bands at ~1090 and ~1020 cm^{-1} were attributed to the absorptions of Si—O—Si and Si—O—Al, respectively (Madejová, 2003). Whether or not the ~1090 cm^{-1} band appeared depended on the content of Al^{3+} in the tetrahedron (Zhang et al., 1990). The band at 779 cm^{-1} was corresponded to trioctahedral chlorite (Zhao and He, 2016). Fig. 4 showed that there were more Si^{4+} substituted by Al^{3+} in the tetrahedron of samples 1-550-265-KCl-24 and 1-550-280-KCl-24. Trioctahedral chlorite had appeared in those two products, however, there was no indication of the reflection of chlorite in sample of 1-550-265-KCl-24, possibly due to the small amount.
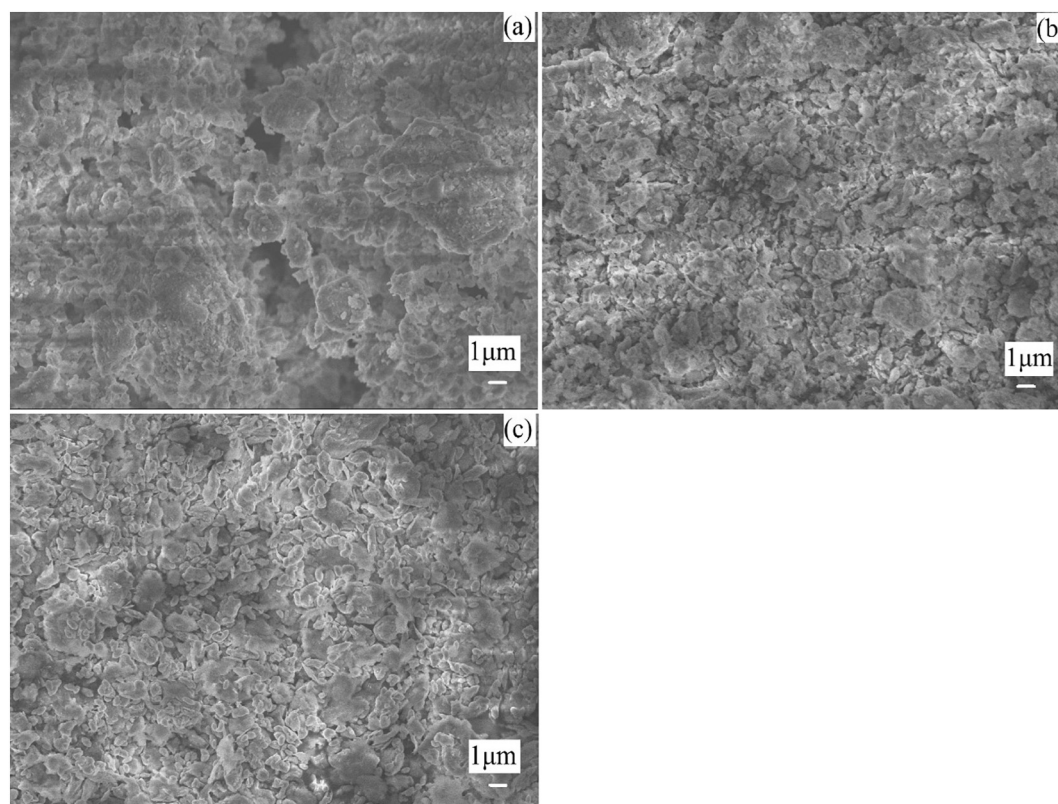
3.5. HRTEM analysis

The illite, I/S and chlorite clays were characterized by lattice-fringe spacings of 1.0, 2.2 and 1.4 nm under HRTEM observation (Fig. 5). Most of the lattice fringes were straight and 1.0 nm thick, consistent with illite layers. At the same time in some particles, the 2.2 nm thick wavy layers rarely existed simultaneously. The former may be interpreted as illite layers (Fig. 5a), while the latter as I/S layers (Fig. 5b). 1.4 nm thick wavy layers also exist in some particles (Fig. 5c), and may be interpreted as chlorite layers. Confirmed by the XRD patterns (Fig. 1f), the dominant clay minerals in the sample of 1-550-280-KCl-24 are chlorite and illite dominant illite/smectite.

3.6. Molecular simulations

The experimental results as mentioned above proved that mixed-layer mineral I/S and newly formed mineral chlorite were present. In this work, molecular modeling and molecular simulation were introduced to simulate the mineral and structure changes. However, the modeling of interstratified illite and smectite layers are beyond the scope of this work because I/S models are too large and would require a high-computational effort. Therefore, the crystal structure models of smectite, illite and chlorite were built and XRD patterns were calculated for the purposes of comparison with experimental patterns.

Based on the lattice parameters of smectite, illite and chlorite, the initial structures were created. The interlayer and tetrahedral cations of

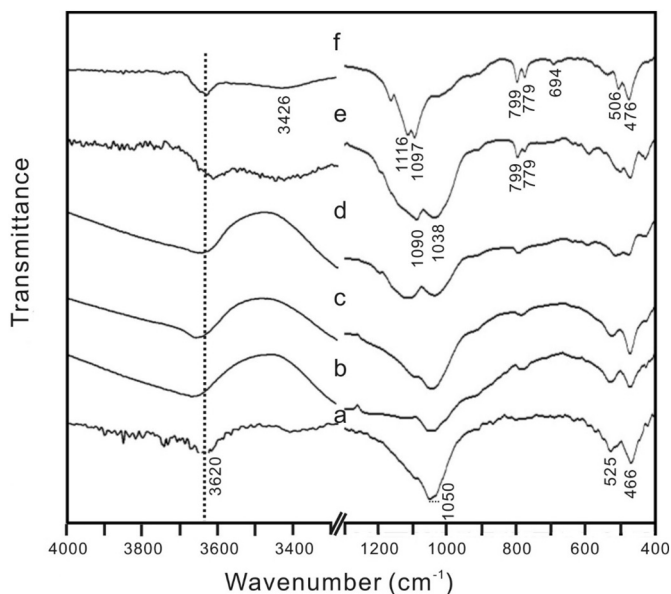**Fig. 3.** SEM images of sample (a) 1-YY, (b) 1-550-265-KCl-24, (c) 1-550-280-KCl-24.

Fig. 4. The FTIR transmittance spectra of the clay minerals of sample (a) 1-YY, (b) 1-250-5-KCl-24, (c) 1-350-65-KCl-24, (d) 1-450-120-KCl-24, (e) 1-550-265-KCl-24, (f) 1-550-280-KCl-24.

smectite and illite were changed according to previous XRF results of samples of 1-YY and 1-550-265-KCl-24 and were calculated to obtain more stable structures. However, XRF results showed a mixture of chlorite and I/S in the sample of 1-550-280-KCl-24 and it was impossible to distinguish the chemical composition, thus, the initial structure of chlorite was not changed. The MS calculated structures were viewed from [100] direction (Fig. 6) and the powder XRD was compared with our experimental oriented XRD patterns (Fig. 7).

As shown in Fig. 6, three types of structures of clay minerals had been obtained in order to simulate the transformation from smectite to chlorite. When smectite transformed to illite, interlayer water evaporated and was accompanied by the release of Ca^{2+}, Na^+ and the injection of K^+. Smectite and illite with the structure of TOT sheet converted into a brucite sheet, and then accompanied by the chemical modification of the tetrahedral sheets in the immediately adjacent smectite layers, formed a chlorite layer (Robinson et al., 2002). The brucite sheet can also be seen as a newly formed octahedral sheet and the structure of chlorite can be written as TOTO′. Accordingly, the diffraction intensity of the trioctahedral (060) reflection with a d value of 1.546 Å was gradually strengthened with the growth of the brucite

sheet (Fig. 2).

The experimental oriented XRD patterns of smectite and illite dominated illite/smectite (001) band (marked with black circles) were consistent with the simulated powder XRD, with the d value only slightly larger than the simulated ones (Fig. 7a and b). The reason was that there was a little organic matter in the sample 1-YY and a small amount of expansion of the smectite layer in the sample of 1-550-265-KCl-24. In the XRD patterns of the sample 1-550-280-KCl-24, (001), (002), (003) and (004) bands of chlorite (marked with black circles in Fig. 7c) were in accordance with the simulated powder XRD.

4. Discussion

4.1. Mineralogical transformations and sequences

To investigate the clay mineral transformation process in detail, the oriented XRD analysis of raw material and experimental samples were exhibited in Fig. 8. XRD patterns of all AD samples showed the same tendency, e.g., a shift of the 001 reflection towards higher angles (from $d_{001} = 15.82$ Å to $d_{001} = 10.23$ Å), and an asymmetry in this reflection (Fig. 8 (AD)). Such an evolution can be attributed to the effects of a substitution of Na^+ and Ca^{2+} by K^+ together with the presence of mixed layer minerals (illite/smectite), and this substitution was temperature and pressure dependent as shown in Fig. 8 (AD).

Quartz and K-feldspar were also present in the products, as shown in Fig. 8 (AD). The intensities of quartz and feldspar reflections increased significantly with the increasing of temperature and pressure. As indicated by Mosser-Ruck and Cathelineau (2004), quartz and feldspar were byproducts of the transformation from low-charge smectite into high-charge smectite (Mosser-Ruck and Cathelineau, 2004; Savage and Liu, 2015). On the other hand, muscovite disappeared in the reflection labeled d and e in Fig. 8 (AD), and this phenomenon was attributed to the pathway Eq. (1) and that K-feldspar might also form. However, there was no indication of the reflection of Als (Andalusite, as referred to the temperature and pressure), possibly due to the small amount.

$$\text{Muscovite} + \text{quartz} = Al_2SiO_5 \text{ minerals} + \text{K-feldspar} + H_2O \qquad (1)$$

In Fig. 8 (EG), X-ray diffraction patterns of glycolated samples are characterized by large d_{001} reflections between ~10 Å and ~17 Å. For samples of 1-250-5-KCl-24 and 1-350-65-KCl-24, typically the mix layered phases were composed of illite and smectite layers. In the sample of 1-250-5-KCl-24, the d_{001} shifted to ~17 Å and showed an asymmetry, while in the sample of 1-350-65-KCl-24, the d_{001} reflection shifted to low angles and showed a large bulge towards ~13.02 Å, but it did not reach to ~17 Å. In the clay minerals, the disappearance of the reflection with a d value of ~17 Å indicated that the interstratified I/S
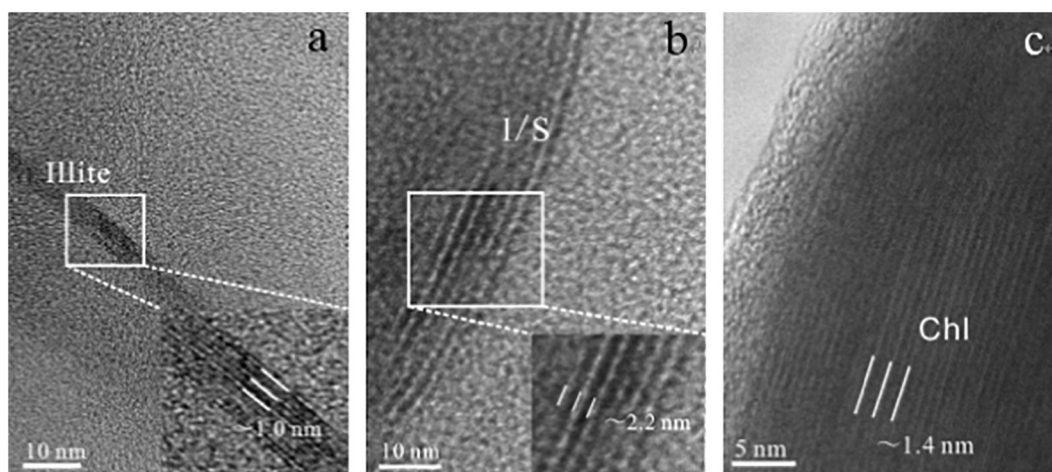

Fig. 5. Lattice fringe image of sample 1-550-280-KCl-24, illite (a), illite/smectite (b) and chlorite (c).
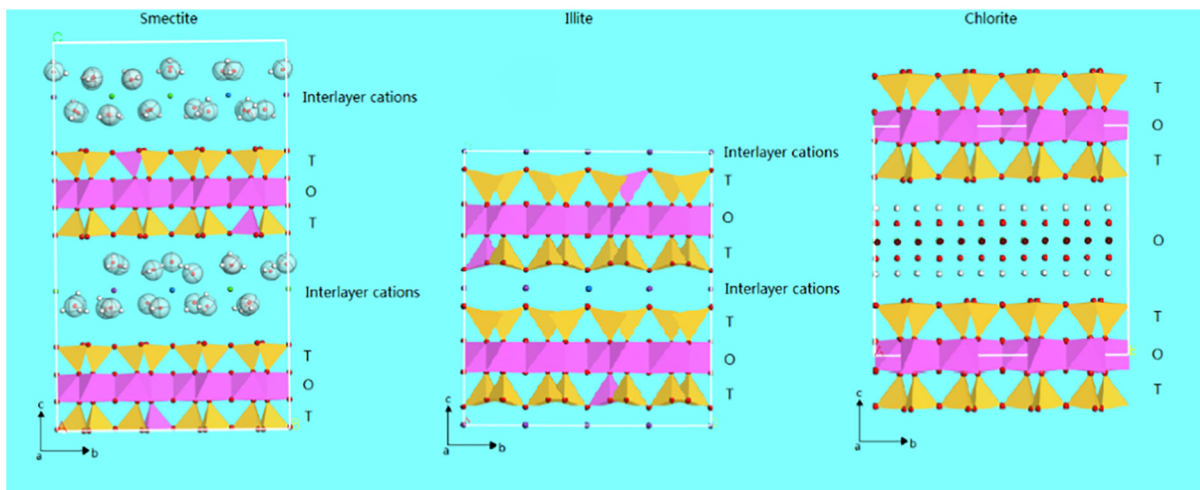
Fig. 6. Schematic diagram to show structures involved in the transformation of smectite to chlorite interstratified minerals, viewing the structures of smectite, illite and chlorite along the [100] direction. (Color code: Ca, green; Si, yellow; H, white; Al, pink; K, purple; Na, blue; Mg, brown; O, red.) (For interpretation of the references to color in this figure legend, the reader is referred to the web version of this article.)
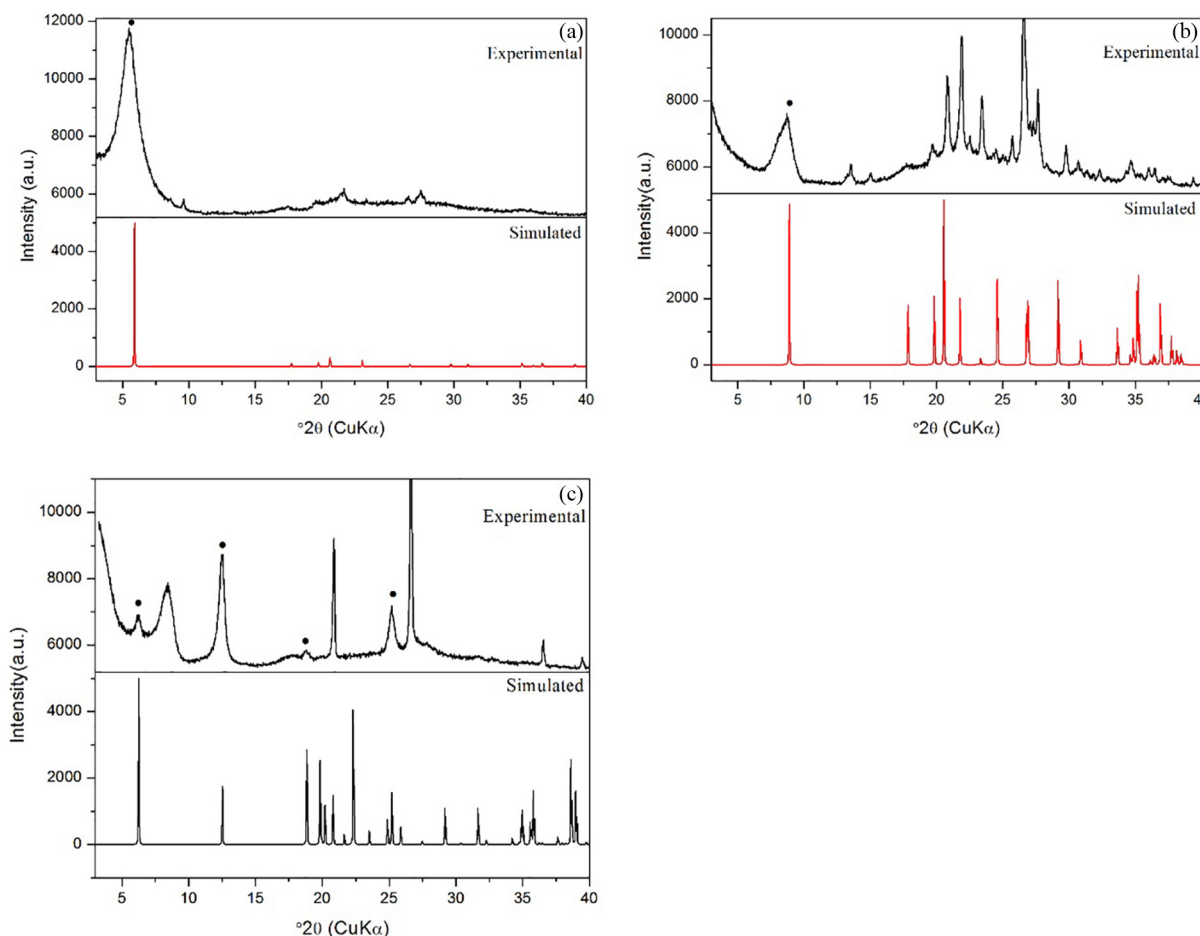

Fig. 7. Simulated and experimental oriented powder XRD patterns of (a)-smectite, (b)-illite, and (c)-chlorite. The smectite and illite dominated illite/smectite (001) band, and chlorite minerals (001), (002), (003), (004) bands marked with black circles.

minerals transformed from a disordered state to an ordered state. These results indicated that sample 1-250-5-KCl-24 was disordered I/S interstratified minerals, while the ordered I/S interstratified minerals formed in the sample of 1-350-65-KCl-24. The portion of smectite which irreversibly collapsed to ~10 Å, can be assigned to the high-charge smectite layers (Howard and Roy, 1985). In the X-ray diffraction patterns of sample 1-550-265-KCl-24, a high reflection at ~10 Å could be assigned to the illite layer. Considering the reflection at ~10 Å is clearly abreast of the lower angle reflection of ~10.23 Å, and after ethylene glycol saturation, the reflection shifted slightly to lower 2θ angles, this phenomenon was caused by the existence of a small amount of smectite in the interlayer of illite.
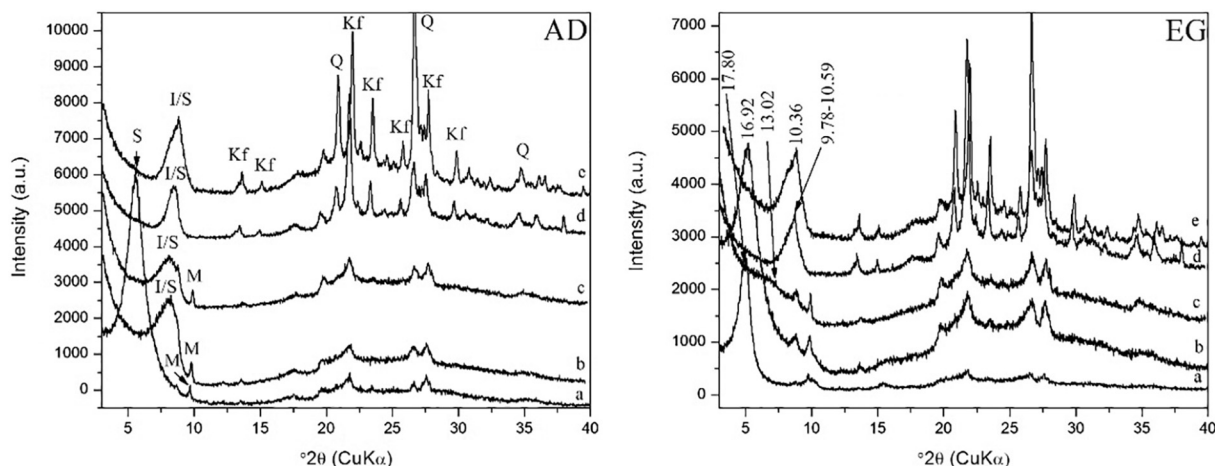
Fig. 8. XRD patterns using Cu Kα radiation for < 2 μm fractions for the samples of (a) 1-YY, (b) 1-250-5-KCl-24, (c) 1-350-65-KCl-24, (d) 1-450-120-KCl-24, (e) 1-550-265-KCl-24,in air-dried (AD) and ethylene glycol (EG) modes, respectively. The main diffraction of (001) bands of sample patterns are labeled in Å. S-smectite, I/S-illite/smectite, M-muscovite, Kf-K-feldspar, Q-quartz.

After investigation of sample 1-550-280-KCl-24, the d_{001} value of reflection was 14.12 Å, and it didn't expand after ethylene glycolation. After heating to 550 °C, the intensities of chlorite peaks were modified. The second, third and fourth peaks of chlorite reflection were diminished (Fig. 1f), these phenomena indicated that a chlorite mineral was formed. No regular interstratified corrensite and chlorite/smectite particles were observed in our simulation.

With the combined investigation of XRD, FTIR and HRTEM, our experiments revealed a continuous evolution from smectite to chlorite throughout the dioctahedral smectite to dioctahedral randomly interstratified I/S to dioctahedral ordered interstrification I/S then to co-existence of dioctahedral and trioctahedral ordered I/S and finally to trioctahedral chlorite and I/S. Similar results were found in previous work (Pelayo et al., 2016). The comparison between this work and other studies (Burst, 1969; Perry Jr and Hower, 1972; Abid et al., 2004; Kang et al., 2012) indicated that this experimental transformation of smectite to I/S interstratified minerals was consistent with the clay mineral transformations that happened in diverse earth crust environments. At the same time, trioctahedral chlorite appearing as a result of higher temperatures and pressures can be attributed to the high reactivity of Fe^{2+} or Mg^{2+} cations. Indications are that octahedral vacancies decreased with increasing temperature, and the increase of trioctahedral character with temperature is a classical feature (Bourdelle et al., 2013; Fernández et al., 2014).

In order to clearly understand the proportional changes, the relative proportions of clay minerals in the experimental samples were determined by the Petroleum Industrial Standards No. SY/T5163-2010 and Srodon (1984). By the oriented AD and EG patterns of XRD, the percentage of smectite layers (S%) in disordered interstratified I/S was determined by Saddle/Peak (S_a/P) and I/(I/S), while the percentage of smectite layers in ordered interstratified I/S was determined by the d value of 10–15 Å. Sa/P was calculated on the diffraction peak of 1.70 nm in EG slide and it represents the rate between the distance of saddle to baseline and peak to baseline. I/(I/S) means the content rate between illite and illite/smectite (Zhao and He, 2016). As shown in Fig. 9a, a schematic illustration of illite percentage (I% = 1 − S%) in illite/smectite interstratified minerals and the structural transformation of illite/smectite interstratified minerals took the temperature and pressure states into account. With the increasing temperature and pressure, the layer of illite increased (transforming from 37% to 94%) in the interstratified mineral I/S, and the structure of I/S transformed from a disordered to an ordered state at 350 °C and the pressure of 65 MPa. The octahedral structure of the clay minerals underwent a structural transformation from a dioctahedral to a mixture of di- and tri-octahedral structures and finally to a trioctahedral dominated structure. As for the sample of 1-550-280-KCl-24, the ratio of chlorite was calculated by using Schultz correct method (Zhao and He, 2016), and the percentage of I/S (39%), were shown in Fig. 9b.

4.2. Temperature conditions for the existence of chlorite

Many studies have been conducted about the formation and stability of illite-smectite (Wu et al., 1975; Ji et al., 1997; Agard et al., 1999; Day-Stirrat et al., 2010), but only a few investigations have been done on the existence and stability of chlorite minerals (Schiffman and Staudigel, 1995). As reported by Suchecki and Kristmannsdottir, in the hydrothermal systems, chlorite-smectite can form at temperatures as high as 250 or 300 °C (Suchecki et al., 1977; Kristmannsdottir, 1979), and in a stable state, chlorite appears at a wide range of temperature, from 110 °C and 420 °C (Iijima and Matsumoto, 1982; Cathelineau and Izquierdo, 1988; Hillier and Velde, 1992; Buatier et al., 1993; Aagaard et al., 2000). In this experiment, the temperature and pressure required for chlorite to appear is 550 °C and 280 MPa, and there were also some smectite layers in the illite (Figs. 1f and 5b). These conditions are considerably greater than the stability depth for smectite suggested by Holdsworth, who only considered the thermal stability of pure smectite, such as saponite (Holdsworth et al., 2011), and not that of the mixed-layer composition in this study. Nevertheless, our simulation experiments only took 24 h and achieved chlorite, which is over a much shorter timescale compared to burial or a very low-grade or low-grade metamorphism history and should be considered.

4.3. Reaction pathways for the smectite-to-illite and smectite-to-chlorite transformations

Comparing the mineralogical and geochemical processes of several reaction mechanisms for smectite illitization, three mechanisms were proposed: 1) solid-state transformation (SST), 2) dissolution and crystallization (DC) and 3) Ostwald ripening (OR) (Altaner and Ylagan, 1997). The SEM images (Fig. 3), clearly showed the dissolvation of smectite grains and the formation of the small illite/smectite and chlorite interstratified minerals, which indicated that the dissolution and crystallization mechanism played a major role in our work (Ylagan et al., 2000; Ferrage et al., 2011).

The transformation from smectite to chlorite has been interpreted as involving either a disequilibrium chlorite/smectite mixed-layering sequence, or an equilibrated discontinuous sequence involving smectite-corrensite-chlorite (Robinson et al., 2002). As indicated by Robinson,
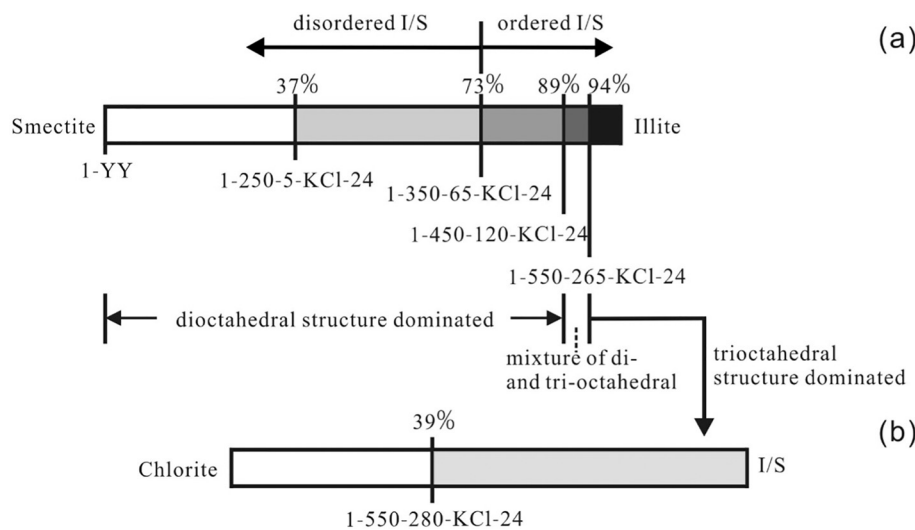
Fig. 9. Schematic diagram to show clay mineral composition and octahedral structure changes as the increasing temperature and pressure. (a) Illite layer ratio in the interstratified mineral I/S increased as the increasing of temperature and pressure, and the structure changed from dioctahedral to trioctahedral. (b) Proportions of C and I/S of sample 1-550-280-KCl-24.

there were three contrasting reaction pathways: (i) a continuous mixed-layer chlorite/smectite series; (ii) a discontinuous smectite-corrensite-chlorite series and (iii) a direct smectite to chlorite transformation. The reaction pathways for the smectite-to-chlorite transformation in this paper can be attributed to a direct smectite to chlorite transformation. Zhang et al. (2010) indicated that increasing rates of growth, relative to nucleation, promoted the generation of more ordered structures and eventually led to the direct smectite to chlorite transition (Zhang et al., 2010).

4.4. Fluid-rock interaction processes for the formation of chlorite

The presence of Mg cations was essential to form the brucite layer for the formation of chlorite in this experiment. The reason why chlorite rather than chlorite-smectite or corrensite formed was related not only to the temperature, but also to the activity of Mg cations within the reactive fluid and the mechanism of formation (Bettison-Varga and MacKinnon, 1997). Chlorite can form directly from solutions or as a replacement product of minerals, whereas chlorite-smectite formed primarily by replacing preexisting clay minerals or another mineral phase (Murakami et al., 1999; Leoni et al., 2010). We did not observe any randomly interstratified chlorite-smectite by XRD and HRTEM, or any layer terminations of the hydroxides found in chlorite minerals. These results indicated that interstratified structure did not form. The direct conversions of smectite to chlorite (at 550 °C 280 MPa, L/S = 1:1 in this experiment), without forming significant amounts of chlorite-smectite observed in the present study, suggests the interstratification is much less stable (Murakami et al., 1999). Schiffman and Staudigel (1995) attribute the absence of randomly interstratified C/S to systematically high, integrated fluid fluxes through rocks.

The mineral phases in the prepared sample 1-550-280-KCl-24 contained chlorite and I/S interstratified minerals. It implied that a range of stable clay minerals can form down to greater depths than illite-smectite interstratified minerals. Based on today's geothermal gradient of 25–35 °C/km and the stability of chlorite, the formation of chlorite minerals may occur as deep as 14–20 km where the activity of Mg is appropriately high (Schleicher et al., 2012). Therefore, chlorite minerals are formed by the high reactivity of Fe or Mg cations, and the substitute isomorphism among the cations. In the diagenetic stage, the source of Fe and Mg is associated with the decomposition of biotite, or the release of Fe and Mg in the conversion process of mixed-layer transformation (Science and Technology Development Department, CNPC, 1999) there are Mg and Fe ions in starting sample 1-YY from its analysis of XRF. However, there is no indication of biotite in the starting raw rock as shown by XRD. Hence, the formation of chlorite minerals

was attributed to ion exchange in the clay minerals structures.

In short, the formation of higher temperature-pressure conditions and the behavior of chlorite phases have not been extensively studied yet, especially at depths or temperature-pressure regions where illite-smectite is not expected to be stable. The stability of Mg-rich chloritic clays at higher temperature-pressure conditions offers a possible explanation for fault weakness at depth (Schleicher et al., 2012), pointing out the direction for future experimental and analytical studies. In recent years, it has been more and more recognized that the clay minerals may be playing an important role in fault weakening behavior and the frictional behavior of smectite-chlorite phases has not yet been extensively studied. Hence, in the study of fault zones, we still need a lot of field observations, and obtain more natural clay minerals to analyze the composition variations. Furthermore, laboratory experiments performed at appropriate temperatures and pressures on clay minerals are needed, which would require artificial samples rather than natural samples. To clarify the influence of organic matter, muscovite, quartz, kaolinite and feldspar et al. on the transformation of clay minerals, pure smectite should be selected as the starting material. And the comparative study of the field samples and experimental ones would be effective way to study the clay mineral transformation. Therefore, this work provided new insights into frictional properties by recognizing the importance of smectite-chlorite clay minerals.

5. Conclusion

In this study, a continuous alteration and reaction progress of clay minerals was obtained under hydrothermal conditions, from dioctahedral smectite to dioctahedral randomly interstratified I/S to dioctahedral ordered interstrification I/S to coexistence of dioctahedral and trioctahedral ordered I/S and finally to trioctahedral chlorite and I/S. As the temperature and pressure increase, the illite layer percentage increased significantly. The reaction pathway for the transition smectite to illite-smectite shown in this work was dissolution and crystallization, and a discontinuous pathway for the transition of smectite to chlorite. The conditions for the formation of chlorite was 550 °C and 280 MPa (in the depth of 14–20 km, calculated on today's geothermal gradient of 25–35 °C/km), where the activity of Mg is appropriately high. Finally, based on the element analysis of XRF, molecular simulation is an effective way to show the structural changes of clay minerals directly. Our findings suggest that laboratory experiments are an effective way to avoid the influence of variable geochemical conditions, a uniform heat-flow and minor tectonic-structural complexity and provide new insights into alteration and reaction progress of clay minerals.

References

Aagaard, P., Jahren, J.S., Harstad, A.O., Nilsen, O., Ramm, M., 2000. Formation of grain-coating chlorite in sandstones. Laboratory synthesized vs. natural occurrences. Clay Miner. 35, 261–269.

Abid, I.A., Hesse, R., Harper, J.D., 2004. Variations in mixed-layer illite/smectite diagenesis in the rift and post-rift sediments of the Jeanne d'Arc Basin, Grand Banks offshore Newfoundland, Canada. Can. J. Earth Sci. 41, 401–429.

Agard, P., Jullien, M., Goffe, B., Baronnet, A., Bouybaouene, M., 1999. TEM evidence for high-temperature (300 degrees C) smectite in multistage clay-mineral pseudomorphs in pelitic rocks (Rif, Morocco). Eur. J. Mineral. 11, 655–668.

Altaner, S.P., Ylagan, R.F., 1997. Comparison of structural models of mixed-layer illite/smectite and reaction mechanisms of smectite illitization. Clay Clay Miner. 45, 517–533.

Bettison, L.A., Schiffman, P., 1988. Compositional and structural variations of phyllosilicates from the Point Sal ophiolite, California. Am. Mineral. 73, 62–76.

Bettison-Varga, L., MacKinnon, I.D., 1997. The role of randomly mixed-layered chlorite/smectite in the transformation of smectite to chlorite. Clay Clay Miner. 45, 506–516.

Bevins, R.E., Robinson, D., Rowbotham, G., 1991. Compositional variations in mafic phyllosilicates from regional low-grade metabasites and application of the chlorite geothermometer. J. Metamorph. Geol. 9, 711–721.

Bourdelle, F., Parra, T., Beyssac, O., Chopin, C., Vidal, O., 2013. Clay minerals as geothermometer: a comparative study based on high spatial resolution analyses of illite and chlorite in Gulf Coast sandstones (Texas, USA). Am. Mineral. 98, 914–926.

Boyle, J., 2004. A comparison of two methods for estimating the organic matter content of sediments. J. Paleolimnol. 31, 125–127.

Bradbury, K.K., Evans, J.P., Chester, J.S., Chester, F.M., Kirschner, D.L., 2011. Lithology and internal structure of the San Andreas fault at depth based on characterization of Phase 3 whole-rock core in the San Andreas Fault Observatory at Depth (SAFOD) borehole. Earth Planet. Sci. Lett. 310, 131–144.

Brindley, G., Brown, G., 1980. Crystal structure of clay minerals and their X-ray identification. In: Mineralogical Society of London Monograph. Mineralogical Society, London.

Buatier, M., Ouyang, K., Sanchez, J., 1993. Iron in hydrothermal clays from the Galapagos spreading centre mounds: consequences for the clay transition mechanism. Clay Miner. 28, 641–656.

Burst, J.F., 1969. Diagenesis of Gulf Coast clayey sediments and its possible relation to petroleum migration. AAPG Bull. 53, 73–93.

Cathelineau, M., Izquierdo, G., 1988. Temperature — composition relationships of authigenic micaceous minerals in the Los Azufres geothermal system. Contrib. Mineral. Petrol. 100, 418–428.

Chang, H.K., Mackenzie, F.T., Schoonmaker, J., 1986. Compositional between the diagenesis of dioctahedral and trioctahedral smectite, Brazilian offshore basins. Clays Clay Miner. 34, 407–423.

Cuadros, J., 2012. Clay crystal-chemical adaptability and transformation mechanisms. Clay Miner. 147.

Day-Stirrat, R.J., Milliken, K.L., Dutton, S.P., Loucks, R.G., Hillier, S., Aplin, A.C., Schleicher, A.M., 2010. Open-system chemical behavior in deep Wilcox Group mudstones, Texas Gulf Coast, USA. Mar. Pet. Geol. 27, 1804–1818.

Dong, H., Peacor, D.R., Merriman, R.J., Kemp, S.J., 2002. Brinrobertsite: a new R1 interstratified pyrophyllite/smectite-like clay mineral: characterization and geological origin. Mineral. Mag. 66, 605–617.

Dubacq, B., Vidal, O., Lewin, É., 2011. Atomistic investigation of the pyrophyllitic substitution and implications on clay stability. Am. Mineral. 241.

Eberl, D., 1978. Reaction series for dioctahedral smectites. Clay Clay Miner. 26, 327–340.

Eberl, D., Whitney, G., Khoury, H., 1978. Hydrothermal reactivity of smectite. Am. Mineral. 63, 401–409.

Fernández, R., Ruiz, A.I., Cuevas, J., 2014. The role of smectite composition on the hyperalkaline alteration of bentonite. Appl. Clay Sci. 95, 83–94.

Ferrage, E., Vidal, O., Mosser-Ruck, R., Cathelineau, M., Cuadros, J., 2011. A reinvestigation of smectite illitization in experimental hydrothermal conditions: results from X-ray diffraction and transmission electron microscopy. Am. Mineral. 96, 207–223.

Gualtieri, A.F., Ferrari, S., Leoni, M., Grathoff, G., Hugo, R., Shatnawi, M., Paglia, G., Billinge, S., 2008. Structural characterization of the clay mineral illite-1M. J. Appl. Crystallogr. 41, 402–415.

Hillier, S., Velde, B., 1992. Chlorite interstratified with a 7 Å mineral: an example from offshore Norway and possible implications for the interpretation of the composition of diagenetic chlorites. Clay Miner. 27, 475–486.

Holdsworth, R.E., van Diggelen, E.W.E., Spiers, C.J., de Bresser, J.H.P., Walker, R.J., Bowen, L., 2011. Fault rocks from the SAFOD core samples: implications for

weakening at shallow depths along the San Andreas Fault, California. J. Struct. Geol. 33, 132–144.

Hong, H., Churchman, G.J., Yin, K., Li, R., Li, Z., 2014. Randomly interstratified illite–vermiculite from weathering of illite in red earth sediments in Xuancheng, southeastern China. Geoderma 214-215, 42–49.

Howard, J.J., Roy, D.M., 1985. Development of layer charge and kinetics of experimental smectite alteration. Clay Clay Miner. 33, 81–88.

Iijima, A., Matsumoto, R., 1982. Berthierine and chamosite in coal measures of Japan. Clay Clay Miner. 30, 264–274.

Inoue, A., Utada, M., 1991. Smectite-to-chlorite transformation in thermally metamorphosed volcanoclastic rocks in the Kamikita area, Northern Honshu, Japan. Am. Mineral. 76, 628–640.

Inoue, A., Utada, M., Nagata, H., Watanabe, T., 1984. Conversion of trioctahedral smectite to interstratified chlorite/smectite in Pliocene acidic pyroclastic sediments of the Ohyu district, Akita Prefecture, Japan. Clay Sci. 6, 103–116.

Ji, J.F., Browne, P.R.L., Liu, Y.J., 1997. Occurrence of mixed-layer illite/smectite at temperature of 285 °C in an active hydrothermal system and its significance. Chin. Sci. Bull. 42, 318–321.

Kameda, J., Ujiie, K., Yamaguchi, A., Kimura, G., 2011. Smectite to chlorite conversion by frictional heating along a subduction thrust. Earth Planet. Sci. Lett. 305, 161–170.

Kang, I.-M., Hillier, S., Song, Y., Kim, I.-J., 2012. Relative coherent stacking potential of fundamental particles of illite-smectite and its relationship to geological environment. Clay Miner. 319.

Kristmannsdottir, H., 1979. Alteration of basaltic rocks by hydrothermal-activity at 100–300°C. In: Mortland, M.M., Farmer, V.C. (Eds.), Developments in Sedimentology. Elsevier, pp. 359–367.

Leoni, L., Lezzerini, M., Battaglia, S., Cavalcante, F., 2010. Corrensite and chlorite-rich Chl-S mixed layers in sandstones from the 'Macigno' Formation (northwestern Tuscany, Italy). Clay Miner. 87.

Madejová, J., 2003. FTIR techniques in clay mineral studies. Vib. Spectrosc. 31, 1–10.

Merriman, R.J., Peacor, D.R., 1999. Very Low-grade Metapelites: Mineralogy, Microfabrics and Measuring Reaction Progress. Blackwell Publishing Ltd, Oxford, UK.

Mosser-Ruck, R., Cathelineau, M., 2004. Experimental transformation of Na,Ca-smectite under basic conditions at 150 °C. Appl. Clay Sci. 26, 259–273.

Murakami, T., Sato, T., Inoue, A., 1999. HRTEM evidence for the process and mechanism of saponite-to-chlorite conversion through corrensite. Am. Mineral. 1080.

Pelayo, M., García-Romero, E., Labajo, M.A., Pérez del Villar, L., 2016. Evidence of montmorillonite/Fe- rich smectite transformation in the Morrón de Mateo bentonite deposit (Spain): implications for the clayey barrier behaviour. Appl. Clay Sci. 131, 59–70.

Perry Jr., E.A., Hower, J., 1972. Late-stage dehydration in deeply buried pelitic sediments. AAPG Bull. 56, 2013–2021.

Robinson, D., Zamora, A., 1999. The smectite to chlorite transition in the Chipilapa geothermal system, El Salvador. Am. Mineral. 84, 607–619.

Robinson, D., Schmidt, S.T., De Zamora, A.S., 2002. Reaction pathways and reaction progress for the smectite-to-chlorite transformation: evidence from hydrothermally altered metabasites. J. Metamorph. Geol. 20, 167–174.

Savage, D., Liu, J., 2015. Water/clay ratio, clay porosity models and impacts upon clay transformations. Appl. Clay Sci. 116-117, 16–22.

Schiffman, P., Staudigel, H., 1995. The smectite to chlorite transition in a fossil seamount hydrothermal system: the Basement Complex of La Palma, Canary Islands. J. Metamorph. Geol. 13, 487–498.

Schleicher, A.M., van der Pluijm, B.A., Solum, J.G., Warr, L.N., 2006. Origin and significance of clay-coated fractures in mudrock fragments of the SAFOD borehole (Parkfield, California). Geophys. Res. Lett. 33, 1–5.

Schleicher, A.M., Van der Pluijm, B.A., Warr, L.N., 2010. Nanocoatings of clay and creep of the San Andreas fault at Parkfield, California. Geology 38, 667–670.

Schleicher, A.M., van der Pluijm, B.A., Warr, L.N., 2012. Chlorite-smectite clay minerals and fault behavior: new evidence from the San Andreas Fault Observatory at Depth (SAFOD) core. Lithosphere 4, 209–220.

Science and Technology Development Department, CNPC, 1999. Chinese Oil and Gas Reservoir Research Collection. Petroleum Industry Press, Beijing, pp. 28 (in Chinese).

Srodon, J., 1980. Precise identification of illite/smectite interstratifications by X-ray powder diffraction. Clay Clay Miner. 28, 401.

Srodon, J., 1984. X-ray powder diffraction identification of illite materials. Clay Clay Miner. 32, 337–349.

Suchecki, R.K., Perry, E., Hubert, J., 1977. Clay petrology of Cambro-Ordovician continental margin, Cow Head Klippe, western Newfoundland. Clay Clay Miner. 25, 163–170.

Velde, B., Suzuki, T.t., Nicot, E., 1986. Pressure-temperature-composition of illite/smectite mixed-layer minerals: Niger delta mudstones and other examples. Clay Clay Miner. 34, 435–441.

Viani, A., Gualtieri Alessandro, F., Artioli, G., 2002. The nature of disorder in montmorillonite by simulation of X-ray powder patterns. Am. Mineral. 966.

Vidal, O., Dubacq, B., 2009. Thermodynamic modelling of clay dehydration, stability and compositional evolution with temperature, pressure and H$_2$O activity. Geochim. Cosmochim. Acta 73, 6544–6564.

Watanabe, T., 1981. Identification of illite/montmorillonite interstratifications by X-ray powder diffraction. J. Mineral. Soc. 15, 32–41.

Watanabe, T., 1988. The structural model of illite/smectite interstratified mineral and the diagram for its identification. Clay Sci. 7, 97–114.

Wu, F.T., Blatter, L., Roberson, H., 1975. Clay gouges in the San Andreas Fault System and their possible implications. In: Wyss, M. (Ed.), Earthquake Prediction and Rock Mechanics. Birkhäuser Basel, Basel, pp. 87–95.

Yamada, H., Y, K., Tamura, K., et al., 1998. Reaction sequence of sodium montmorillonite under hydrothermal conditions. Clay Sci. 10, 385–394.

Ylagan, R.F., A, S.P., Pozzuoli, A., 2000. Reaction mechanisms of smectite illitization associated with hydrothermal alteration from Ponza Island, Italy. Clay Clay Miner. 48, 610–631.

Zhang, N.X., Li, Y.Q., Zhao, H.M., Ji, S.R., 1990. Research Methods of Clay Minerals. Science Press, Beijing, pp. 127–129 (in Chinese).

Zhang, D., Zhou, C.H., Lin, C.X., Tong, D.S., Yu, W.H., 2010. Synthesis of clay minerals.

Appl. Clay Sci. 50, 1–11.

Zhao, X.Y., He, D.B., 2016. Clay Mineral and Application in Oil and Gas Exploration and Development. Petroleum Industry Press, Beijing (pp. 49, 58–63, 92–107, in Chinese).

Zheng, H., Bailey, S.W., 1989. Structures of intergrown triclinic and monoclinic IIb chlorites from Kenya. Clay Clay Miner. 37, 308–316.